


Cite this: *RSC Adv.*, 2020, 10, 8055

# Effect of Fe, Co and Ni promoters on MoS<sub>2</sub> based catalysts for chemoselective hydrogenation of nitroarenes†

Wenpeng Han,<sup>a</sup> Shanmin Wang,<sup>c</sup> Xuekuan Li,<sup>a</sup> Ben Ma,<sup>a</sup> Mingxian Du,<sup>a</sup> Ligong Zhou,<sup>a</sup> Ying Yang,<sup>a</sup> Ye Zhang<sup>a</sup> and Hui Ge<sup>\*a</sup>

The effect of Fe, Co and Ni promoters on supported MoS<sub>2</sub> catalysts for hydrogenation of nitroarenes were systematically investigated *via* experiment, characterization and DFT calculation. It was found that the addition of promoters remarkably improved the reaction activity in a sequence of Ni > Co > Fe > Mo. Meanwhile Ni promoted catalyst with the best performance showed good recyclability and chemoselectivity for a wide substrate scope. The characterization results revealed that the addition of promoters decreased the interaction between Mo and support and facilitated the reductive sulfidation of Mo species to produce more coordinated unsaturated sites (CUS). DFT calculations showed that the addition of promoters increased the formation of CUS, and enhanced the adsorption of hydrogen. The influence degree of promoters followed the sequence Ni > Co > Fe > Mo, which was consistent with those of the activities. Nitrobenzene hydrogenation and hydrogen activation occurred at the S and Mo edge, respectively. The adsorbed hydrogen diffused from the Mo edge to the S edge to participate in the hydrogenation reaction. Mechanism investigation showed that the main reason for increased activity by the addition of promoters was the increase of amounts of CUS and the secondary reason was the augmentation of intrinsic activity of CUS. The present studies give a new understanding for promoter modified MoS<sub>2</sub> catalysts applied for hydrogenation of nitroarenes.

Received 12th January 2020  
Accepted 17th February 2020

DOI: 10.1039/d0ra00320d

rsc.li/rsc-advances

## 1 Introduction

Functionalized arylamines, which are primarily synthesized by chemoselective hydrogenation of the corresponding nitroarenes, are important organic intermediates for producing dyestuffs, agrochemicals, polymers, pharmaceuticals, and so on.<sup>1,2</sup> However, the selective reduction of functionalized nitro compounds is challenging due to the presence of other highly reducible groups, such as C=C, C=O and C≡C groups.<sup>3,4</sup> Traditionally, the noble metal (such as Pt, Pd, Ru, Rh, Au, Ag) catalysts have frequently been reported for this transformation, but the viability and cost of noble metals is a major barrier for their industrial applications.<sup>5–9</sup> Thus, the non-noble metal based catalysts including the base metals, their oxides, carbides and sulfides have been extensively studied as the alternatives.<sup>10–17</sup>

As we know, the two dimensional material is a powerful platform to design single site catalysts and its applications in CO<sub>2</sub> reduction, CO oxidation, and so on.<sup>18–22</sup> Among them, transition metal disulfides (TMDs) also attracted widespread attention due to good catalytic performance for hydrogenation of nitroarenes.<sup>23,24</sup> Ma *et al.* found that FeS<sub>2</sub> and graphene-supported CoS<sub>2</sub> catalysts showed good reaction activity for hydrogenation of nitroarenes.<sup>25,26</sup> Wei *et al.* reported that a porous carbon supported CoS<sub>2</sub> catalyst showed a superior selectivity of 99% towards 3-aminostyrene.<sup>27</sup> Duan *et al.* synthesized a novel N, S-codoped porous carbon supported FeS<sub>2</sub> catalyst and exhibited excellent catalytic activity and tolerance for functionalized nitroarenes using water as a solvent.<sup>28</sup> Among the TMDs, molybdenum disulfide (MoS<sub>2</sub>) with the typical graphene-like two dimensional property is emerging as a new catalyst for hydrogenation of nitroarenes.<sup>29–31</sup> For example, commercial MoS<sub>2</sub> and an oxygen-implanted MoS<sub>2</sub> (O-MoS<sub>2</sub>) catalysts have been used to synthesize functionalized anilines from corresponding nitroarenes using hydrazine (N<sub>2</sub>H<sub>4</sub>·H<sub>2</sub>O) as the hydrogen source.<sup>32–34</sup> A MoS<sub>2</sub> nanocatalyst whose interlayer expanded by the insertion of carbon (MoS<sub>2</sub>@C) was reported to exhibit better catalytic performance compared with that of bulk MoS<sub>2</sub> catalyst.<sup>35</sup>

Bulk MoS<sub>2</sub> is a sandwich (S–Mo–S) layered structure composed of covalent bond in the layer and van der Waals in

<sup>a</sup>Institute of Coal Chemistry, Chinese Academy of Sciences, Taiyuan 030001, China

<sup>b</sup>University of Chinese Academy of Sciences, Beijing 100049, China

<sup>c</sup>Department of Physics, Southern University of Science & Technology, Shenzhen, Guangdong, 518055, China

† Electronic supplementary information (ESI) available: Reaction evaluation, catalyst characterization and DFT calculation for NO adsorption on Mo edge. See DOI: 10.1039/d0ra00320d



the interlayer. The catalytic active centers are supposed to be located on the edges of MoS<sub>2</sub>. The catalytic hydrogenation activity can be improved by reducing the particle sizes of MoS<sub>2</sub> to expose more edges or adding metal promoters to form M–Mo–S phase at the edges of MoS<sub>2</sub>.<sup>36</sup>

As an effective method, the promoter modification has been widely used to improve the catalytic performance of MoS<sub>2</sub> in the hydrodesulphurization (HDS) and hydrogen evolution reaction (HER) *etc.*<sup>37</sup> And this promotion effect is mainly ascribed to the addition of promoter can remarkably reduce the binding energy compared with Mo and S at the edges of MoS<sub>2</sub>, which can lead to the formation of more active centers. Recently, Corma's group synthesized the nanolayered Co–Mo–S catalysts by one-pot hydrothermal method.<sup>38</sup> Compared with the pure MoS<sub>2</sub>, Co-promoted MoS<sub>2</sub> showed excellent activity and selectivity for the nitroarenes with reducible groups (such as C=C, C≡C, C=O). Nethravathi *et al.* reported Co-doped MoS<sub>2</sub> nanosheets and applied for the nitroarene reduction.<sup>39</sup> The results showed that incorporation of cobalt ions in the MoS<sub>2</sub> lattice is the major reason for the efficiency of the promoted catalyst.

Although the important role of Co has been evidenced for selective hydrogenation of nitroarenes of MoS<sub>2</sub> based catalysts, other candidate promoters (such as Fe, Ni) have not been studied. And there is lack of sufficient understanding of promoter effect on the structure–activity relationship and reaction mechanism of selective hydrogenation of nitroarenes, which will inhibit the application of MoS<sub>2</sub> based catalysts. Besides, the Al<sub>2</sub>O<sub>3</sub> was considered as a good support and widely used in many hydrogenation reactions.<sup>40</sup> The Al<sub>2</sub>O<sub>3</sub> can not only disperse the active components to improve the catalytic efficiency, but also can promote the promoter effectively adsorbed on the edge of MoS<sub>2</sub> slabs to form more the single active component instead of the mixed active phase, which made the study more simplified. In this work, we systematically compared the effect of Fe, Co and Ni promoters on hydrogenation of nitroarenes over alumina supported MoS<sub>2</sub> based catalysts. Good activity and chemoselectivity by the addition of promoters were evidenced, especially for Ni promoter. By various characterizations, the effect of promoters on the morphology and sulfidation of MoS<sub>2</sub> were revealed. And DFT calculation was used to investigate the effect of promoters on the formation and regeneration of active centers, the adsorption of nitrobenzene and hydrogen, as well as reaction mechanism. The relationship of activity–structure was built based on the understanding of the key role of promoters located at the S edge of MoS<sub>2</sub>.

## 2 Experimental and theoretical methods

### 2.1 Chemicals and reagents

Nickel nitrate hexahydrate (Ni(NO<sub>3</sub>)<sub>2</sub>·6H<sub>2</sub>O, 99.0%), cobalt nitrate hexahydrate (Co(NO<sub>3</sub>)<sub>2</sub>·6H<sub>2</sub>O), ferric nitrate nonahydrate (Fe(NO<sub>3</sub>)<sub>3</sub>·9H<sub>2</sub>O) and ammonium molybdate ((NH<sub>4</sub>)<sub>6</sub>Mo<sub>7</sub>O<sub>24</sub>·4H<sub>2</sub>O) were ordered from Sinopharm Chemical Reagent Co., Ltd. The other nitroarenes were obtained from Aladdin Reagent Co.

### 2.2 General procedure for catalyst preparation

According to the previous reports,<sup>41</sup> MoO<sub>3</sub>/γ-Al<sub>2</sub>O<sub>3</sub> precursor was obtained by impregnation of 5.0 g γ-Al<sub>2</sub>O<sub>3</sub> with 6.5 mL ammonia solution of (NH<sub>4</sub>)<sub>6</sub>Mo<sub>7</sub>O<sub>24</sub>·4H<sub>2</sub>O (1.21 g, AHM), followed by drying at 100 °C for 8 h and calcining under air at 450 °C for 4 h, the content of Mo was determined as about 9.7 wt% by ICP-AES analysis (see Table S2, ESI†). M–MoO<sub>3</sub>/γ-Al<sub>2</sub>O<sub>3</sub> precursor (M = Fe, Co, Ni) was prepared by impregnation of MoO<sub>3</sub>/γ-Al<sub>2</sub>O<sub>3</sub> with an aqueous solution of Ni(NO<sub>3</sub>)<sub>2</sub>·6H<sub>2</sub>O, Co(NO<sub>3</sub>)<sub>2</sub>·6H<sub>2</sub>O, or Fe(NO<sub>3</sub>)<sub>3</sub>·9H<sub>2</sub>O, and then dried at 100 °C for 8 h and calcined under air at 450 °C for 4 h. The contents of promoters and Mo were about 2.3% and 9.7%, respectively. NiO/γ-Al<sub>2</sub>O<sub>3</sub> was synthesized by impregnation of γ-Al<sub>2</sub>O<sub>3</sub> with an aqueous solution of Ni(NO<sub>3</sub>)<sub>2</sub>·6H<sub>2</sub>O and treatment at the above process, and the content of Ni was about 2.3%.

The precursors were activated by sulfidation with dimethyl disulfide (DMDS) before usage. The sulfidation procedure was following: 0.1 g catalyst was ground and sieved to 40–60 mesh, and then loaded in a fixed bed reactor with an inner diameter of 6 mm. The system was pressured to 4.0 MPa, and then heated to 200 °C within 1.5 h in a hydrogen flow (32 mL min<sup>−1</sup>). The 1.5 wt% DMDS dissolved in *n*-nonane (0.08 mL min<sup>−1</sup>) was pumped into the reaction system at 200 °C. The reactor was maintained at 200 °C for 2 h, followed by heating to 350 °C in 1 h, and held at the temperature for 4 h; after that, the reactor was cooled down to 280 °C. After sulfidation, the catalysts were purged with *n*-hexane three times, then dried under Ar atmosphere and sealed in a glass bottle for reactions and characterizations. The sulfided catalysts were denoted as MoS<sub>2</sub>/γ-Al<sub>2</sub>O<sub>3</sub>, M–MoS<sub>2</sub>/γ-Al<sub>2</sub>O<sub>3</sub> (M = Fe, Co, Ni), and NiS<sub>x</sub>/γ-Al<sub>2</sub>O<sub>3</sub>, respectively.

### 2.3 Catalyst characterization

The high-resolution transmission electron microscopy (HRTEM) was performed using a Tecnai G2 F20 S-Twin at an accelerating voltage of 200 kV. The size and stacking number of M (Fe, Co, Ni)–MoS<sub>2</sub> crystallites were counted over more than 400 particles from ten electron microscope photos.

X-ray photoelectron spectroscopy (XPS) was performed on a Kratos AXIS ULTRA DLD spectrometer with Al K<sub>α</sub> radiation and a multichannel detector, the binding energies were referenced to the C 1s at 284.6 eV.

The Ni and Mo content were determined by inductively coupled plasma-atomic emission spectrometry (ICP-AES) using an iCPA6300 instrument (Thermo Electron, USA).

Temperature-programmed reduction (TPR) measurements were carried out on a TP-5080 (Tianjin-Xianquan, China) quartz micro reactor equipped to a thermal conductivity detector (TCD). About 50 mg of oxidized precursor was heated from room temperature up to 850 °C at 10 °C min<sup>−1</sup> with 5% H<sub>2</sub>–95% N<sub>2</sub> (30 mL min<sup>−1</sup>) and held at that the temperature for 5 min.

Temperature-programmed desorption measurements of NO (NO-TPD) of sulfided catalysts were also carried out on this TP-5080. To avoid possible oxidation of catalysts, the samples (~100 mg) were pretreated at 575 K for 30 min in H<sub>2</sub>, which was saturated by DMDS in a bubble device at ambient temperature,



followed by cooling the samples to 473 K for 30 min in a He atmosphere with a flow rate of 26 mL min<sup>-1</sup>, and then cooled to 323 K over a period of 60 min. Prior to desorption, adsorption of NO was conducted at 323 K in a 1% NO-99% He atmosphere for 60 min at a flow at 52 mL min<sup>-1</sup>. The catalyst was then flushed in a He flow at 323 K for 60 min with a flow rate of 26 mL min<sup>-1</sup> in order to eliminate the physically adsorbed NO. Desorption of NO was conducted from 323 K to 773 K with a heating rate of 10 K min<sup>-1</sup>. The amount of the desorbed NO was determined by an OmniStar GSD-320 mass spectrometer, which was pre-calibrated using standard mixed gases.

## 2.4 General procedure for hydrogenation of nitroarenes

Typically, substrates (1.0 mmol) and decalin (internal standard, 0.1 g) were injected to 15 mL isopropyl alcohol (IPA). The catalyst (0.1 g) and hydrazine hydrate (N<sub>2</sub>H<sub>4</sub>·H<sub>2</sub>O) were added into the above solution. Then, the reaction mixture was sealed and purged with 1 MPa N<sub>2</sub>. Finally, the reaction was heated to 100 °C at stirring and kept at the temperature for some time. After the reaction, the catalyst was separated and the solution was analyzed by GC and GC-MS.

## 2.5 Density functional theory (DFT) calculations

The first-principles DFT calculations were performed on Vienna *Ab initio* Simulation Package (VASP) using the Perdew–Burke–Ernzerh (PBE) functional of the generalized gradient approximation (GGA) to describe the exchange correlation effects, and the projector augmented waves method to treat the ionic–electronic interaction.

As for the MoS<sub>2</sub> catalyst with or without promoter modification, the active phases are hexagon slabs stacked from one to several layers. According to the literature,<sup>42,43</sup> the coordinated unsaturated sites (CUS) on the edges are the main active centers. In this study, we constructed the 4 × 3 × 1 slab in the supercell with the lattice parameters of 12.664 × 30.053 ×

13.170 Å (Fig. 1). The about 13 Å interval distance between slabs and about 20 Å of the vacuum layer thickness can avoid noticeable interaction between repeated structures.

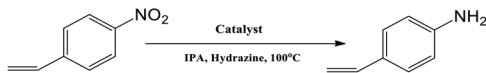
To investigate the effect of promoters, the 100% Mo atoms exposed at Mo and S edges are substituted with Fe, Co or Ni atoms, respectively.<sup>44</sup> Meanwhile the spin was set to the unstrict with the Fe, Co or Ni decoration. In order to save computation time, only atoms above the blue plane in Fig. 1 were kept free move, and all other atoms were frozen. The plane wave based total energy minimization scheme was utilized with a 1 × 2 × 2 *k*-point mesh and 350 eV energy cutoff, structures was relaxed until the force and energy on each atom was converged to less than 0.02 eV Å<sup>-1</sup> and 10<sup>-5</sup> eV. The exploration of transition state (TS) was conducted using the CINEB method with the same convergence standard as the structure optimization, and the TS was verified by the only one imaginary frequency of normal mode of the dynamical matrix.

# 3 Results and discussion

## 3.1 Selective hydrogenation of 4-nitrostyrene over various catalysts

A series of sulfided catalysts were tested for the selective hydrogenation of 4-nitrostyrene with hydrazine hydrate (N<sub>2</sub>H<sub>4</sub>·H<sub>2</sub>O) as reducing agent (Table 1). No transformation was observed in the absence of catalyst (Entry 1). And the product

Table 1 Selective hydrogenation of 4-nitrostyrene over various catalysts<sup>a</sup>

				
Entry	Catalyst	Time (h)	Select <sup>c</sup> (%)	Yield <sup>e</sup> (%)
1	—	1	0	0
2	γ-Al <sub>2</sub> O <sub>3</sub>	1	65	6
3	NiS <sub>x</sub> /γ-Al <sub>2</sub> O <sub>3</sub>	1	77	14
4	MoS <sub>2</sub> /γ-Al <sub>2</sub> O <sub>3</sub>	1	98	50
5	MoS <sub>2</sub> /γ-Al <sub>2</sub> O <sub>3</sub>	2	98	79
6 <sup>b</sup>	O-MoS <sub>2</sub>	2	95	56
7 <sup>c</sup>	MoS <sub>2</sub> /γ-Al <sub>2</sub> O <sub>3</sub>	2	90	<5
8	Fe-MoS <sub>2</sub> /γ-Al <sub>2</sub> O <sub>3</sub>	1	99	52
9	Fe-MoS <sub>2</sub> /γ-Al <sub>2</sub> O <sub>3</sub>	2	97	82
10	Co-MoS <sub>2</sub> /γ-Al <sub>2</sub> O <sub>3</sub>	1	98	65
11	Co-MoS <sub>2</sub> /γ-Al <sub>2</sub> O <sub>3</sub>	2	95	87
12	Ni-MoS <sub>2</sub> /γ-Al <sub>2</sub> O <sub>3</sub>	1	99	95
13	Ni-MoS <sub>2</sub> /γ-Al <sub>2</sub> O <sub>3</sub>	2	98	98
14 <sup>d</sup>	NiS <sub>x</sub> /γ-Al <sub>2</sub> O <sub>3</sub> + MoS <sub>2</sub> /γ-Al <sub>2</sub> O <sub>3</sub>	1	86	63
15 <sup>d</sup>	NiS <sub>x</sub> /γ-Al <sub>2</sub> O <sub>3</sub> + MoS <sub>2</sub> /γ-Al <sub>2</sub> O <sub>3</sub>	2	83	80

<sup>a</sup> Reaction conditions: 0.1 g catalyst, 1 mmol 4-nitrostyrene, 100 °C, 15 mL isopropyl alcohol, 1 MPa N<sub>2</sub>, 3 equiv. N<sub>2</sub>H<sub>4</sub>·H<sub>2</sub>O, calibration concentration of N<sub>2</sub>H<sub>4</sub>·H<sub>2</sub>O is 79.2%. <sup>b</sup> 18 mg catalyst (the molar content of Mo is the same as that of supported catalyst). <sup>c</sup> There was no N<sub>2</sub>H<sub>4</sub>·H<sub>2</sub>O added. <sup>d</sup> 0.2 g catalyst. <sup>e</sup> Detected by GC-MS and GC using decalin as the internal standard.

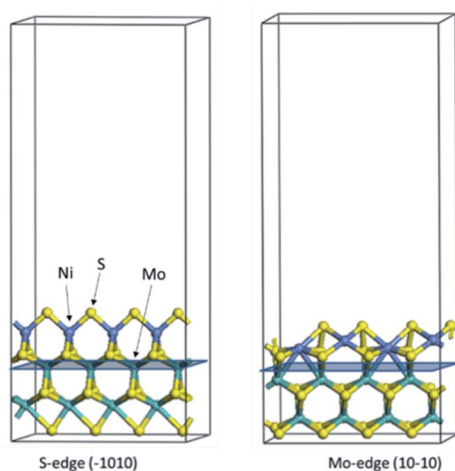


Fig. 1 The periodic model of MoS<sub>2</sub> with S and Mo edges exposed respectively, which is modified by 100% Ni substitution and covered by 50% S atoms. Purple ball, Mo atom; grey ball, Ni atom; yellow ball, S atom.





yield was low using  $\gamma$ - $\text{Al}_2\text{O}_3$  or  $\text{NiS}_x/\gamma$ - $\text{Al}_2\text{O}_3$  as catalysts (Entry 2 and 3). In contrast,  $\text{MoS}_2/\gamma$ - $\text{Al}_2\text{O}_3$  exhibited nearly 100% selectivity and over 50% yield after 2 h (Entry 4 and 5). And the yield was higher than the unsupported O- $\text{MoS}_2$  catalyst (Entry 6) in the literature,<sup>34</sup> which indicated that this supported catalyst improved the catalytic efficiency for the hydrogenation of 4-nitrostyrene. As we known, the IPA was also considered as a reductant or hydrogen source.<sup>45</sup> In order to study the effect of the IPA, the experiment was conducted without  $\text{N}_2\text{H}_4 \cdot \text{H}_2\text{O}$  (Entry 7). There was less than 5% yield obtained, indicating that IPA was not a good reductant or hydrogen source in this catalytic system. The yield was improved by the catalysts with the addition of Fe, Co, or Ni promoters. A slight increase of yield was observed by using Fe promoter modified catalyst (Entry 8 and 9). An apparent increase of yield (from 50% to 65%) was observed by using Co promoter modified catalyst (Entry 10 and 11), however, it is still lower than those of the reported, which may be related to the lower Co loadings. Corma *et al.* also found that when Co/Mo ratio was low (0.17), the activity of the catalyst was significantly reduced.<sup>38</sup> Interestingly, with Ni adding into  $\text{MoS}_2$  catalyst, the yield was improved from 50% to 95% and the selectivity was 99% (Entry 12). When reaction time prolonged to 2 hours, 4-nitrostyrene was completely converted into the 4-aminostyrene (Entry 13). The above results showed that the addition of Ni promoter played crucial role for hydrogenation of nitroarenes. To determine whether the interaction between Ni and  $\text{MoS}_2$  was the reason for improved high activity,  $\text{NiS}_x/\gamma$ - $\text{Al}_2\text{O}_3$  and  $\text{MoS}_2/\gamma$ - $\text{Al}_2\text{O}_3$  catalysts were mechanically mixed and used for the reduction of 4-nitrostyrene (Entry 14 and 15). The yield and selectivity were apparently less than  $\text{Ni-MoS}_2/\gamma$ - $\text{Al}_2\text{O}_3$  catalyst. Thus, the interaction between Ni and  $\text{MoS}_2$  presented important influences, which also was demonstrated by  $\text{H}_2$ -TPR and XPS results (in below).

Encouraged by good performance of  $\text{Ni-MoS}_2/\gamma$ - $\text{Al}_2\text{O}_3$  catalyst, the selective hydrogenation of various nitroarenes were further investigated. The selectivity, yield and optimized conditions are shown in Table S1.† For the halogen-substituted substrates, excellent yields (99%) of the corresponding haloanilines were obtained without any dehalogenation. No matter the substrates with electron-donating substituted groups (such as methyl and amino) or electron-withdrawing substituted groups (such as phenolic hydroxyl, alcoholic hydroxyl, carboxyl and ester) could be reduced to corresponding arylamines with high activity and selectivity. Although nitrile, ketone and olefinic group were supposed to be highly reducible groups, here only corresponding arylamines were obtained while the highly reducible groups were maintained. Because the noble metal and transition metal catalysts are sensitive to sulfur poisoning, the hydrogenation of nitroarenes with sulfur heteroatoms is challenging. In this work, the  $\text{Ni-MoS}_2/\gamma$ - $\text{Al}_2\text{O}_3$  catalyst was sulfur resistant and showed good performance for hydrogenation of the sulfur-containing nitroarenes. The above results showed that the Ni promoted  $\text{MoS}_2$  catalyst exhibited good chemoselectivity for a wide range of substituted nitroarenes. The compatibility for various substrates was also demonstrated for un-promoted and Co promoted  $\text{MoS}_2$  catalysts by the previous reports.<sup>34,38</sup> Our and other researches

suggested that  $\text{MoS}_2$  based catalyst can achieve high selectivity for hydrogenation of nitroarenes. In addition, the reusability and hot filtration tests of the catalyst was also conducted using the nitrobenzene as a model compound to synthesize aniline. Fig. S1 (ESI†) showed that  $\text{Ni-MoS}_2/\gamma$ - $\text{Al}_2\text{O}_3$  catalyst was stable after five consecutive runs.

### 3.2 Catalysts characterization

The morphology and microstructure of the  $\text{MoS}_2$  based catalyst series were observed by the high-resolution transmission electron microscopy (HRTEM). The HRTEM images in Fig. 2a–d clearly showed the generation of typical layered structure with a  $d$ -spacing of 0.65 nm, corresponding to (001) planes of hexagonal  $\text{MoS}_2$  sheets. Compared with  $\text{MoS}_2/\gamma$ - $\text{Al}_2\text{O}_3$ , the addition of the Fe, Co and Ni promoters can decrease slab lengths and increase stacking numbers of  $\text{MoS}_2$  sheets (Fig. 2e and f). The decreased slab lengths suggested high dispersion of active crystallites, which can expose more active edges and thus improve catalytic activity. The increased stacking numbers indicated that the promoters decreased the interaction between Mo and support, facilitating the formation of type II active phase with higher intrinsic activity.<sup>46</sup> Especially, the addition of Ni promoter formed smallest crystallite sizes and highest stacking numbers, which may be one of the reasons for its high catalytic activity. In addition, high-angle annular dark-field scanning TEM (HAADF-STEM) image (Fig. 2g) showed a homogeneous distribution of Ni, Mo and S elements at  $\text{Ni-MoS}_2/\gamma$ - $\text{Al}_2\text{O}_3$  catalyst surface, indicating high dispersion of active particles. From the XRD patterns (Fig. S2, ESI†), no obvious peaks corresponded to  $\text{MoS}_2$  or promoters, which also confirmed the high dispersion of active particles.

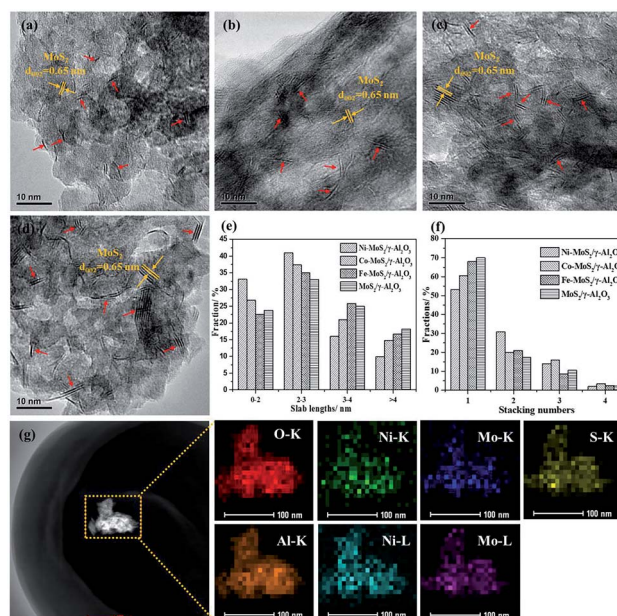


Fig. 2 HRTEM images of  $\text{MoS}_2/\gamma$ - $\text{Al}_2\text{O}_3$  (a),  $\text{Fe-MoS}_2/\gamma$ - $\text{Al}_2\text{O}_3$  (b),  $\text{Co-MoS}_2/\gamma$ - $\text{Al}_2\text{O}_3$  (c),  $\text{Ni-MoS}_2/\gamma$ - $\text{Al}_2\text{O}_3$  (d); the slab lengths (e) and stacking numbers (f) of catalysts; HAADF-STEM images (g) of  $\text{Ni-MoS}_2/\gamma$ - $\text{Al}_2\text{O}_3$  catalyst.



To investigate the reducibility and interaction between promoters and Mo, the  $H_2$ -TPR profiles of calcined  $MoO_3/\gamma-Al_2O_3$ ,  $FeO_x-MoO_3/\gamma-Al_2O_3$ ,  $CoO_x-MoO_3/\gamma-Al_2O_3$  and  $NiO_x-MoO_3/\gamma-Al_2O_3$  samples were presented in Fig. 3. For  $MoO_3/\gamma-Al_2O_3$ , there were two typical reduction peaks located at about 457 °C and 817 °C (Fig. 3a), respectively, corresponding to the reduction peaks of Mo-containing species from  $Mo^{6+}$  to  $Mo^{4+}$  and from  $Mo^{4+}$  to  $Mo^0$ . After adding Fe promoter, the reduction peak (from  $Mo^{6+}$  to  $Mo^{4+}$ ) occurred at higher temperature (about 470 °C) in Fig. 3b and there was no obvious reduction peak of  $FeO_x$ , indicating that there was the interaction between Fe and Mo and the addition of Fe slightly inhibited the reduction of Mo species. After adding Co promoter, the reduction peak of Mo-containing species from  $Mo^{6+}$  to  $Mo^{4+}$  slightly shifted to lower temperature (Fig. 3c). Besides, the TPR peak attributed to molybdate from  $Mo^{4+}$  to  $Mo^0$  also moved to a lower temperature (from 817 °C to 773 °C), indicating that the addition of Co facilitated reduction of Mo species. After adding Ni promoter, the former TPR peak remarkably dropped from 457 °C to 394 °C, and the later TPR peak decreased from 817 °C to 748 °C (Fig. 3d), suggesting the strong promoted effect of Ni on the reduction of Mo species, which may be favorable for the reductive sulfidation of Mo species.

The electronic properties of Mo in pure  $MoS_2$  and Fe, Co and Ni promoted  $MoS_2$  catalysts were investigated using XPS technique in Fig. 4. According to the previous reports,<sup>47</sup> the peaks of binding energies near 229.1, 231.2 and 232.8 eV are attributed to  $Mo^{4+}$ ,  $Mo^{5+}$  and  $Mo^{6+}$  of  $Mo\ 3d_{5/2}$ , and the peak near 226.4 eV is attributed to S 2s. The Mo oxide in the catalyst is +6 valence, and the valence state of Mo will be reduced to +4 and +5 valence after sulfidation. The XPS peaks of Mo in Fig. 4 showed that although the majority of Mo presented in +4 and +5 valence, a part of Mo was still located at +6 valence without sulfidation.

The relative proportion of Mo in different valence states was shown in Table 2. For the Fe, Co and Ni promoted  $MoS_2$  catalysts, the relative contents of  $Mo^{4+}$  were 40.5%, 42.5% and 46.2%, respectively, higher than the  $MoS_2/\gamma-Al_2O_3$  catalyst (38.7%), and the sum of  $Mo^{4+}$  and  $Mo^{5+}$  was also higher than that of the  $MoS_2/\gamma-Al_2O_3$  catalyst, which indicated that the addition of promoters improved the reductive sulfidation of Mo species. And the improved degree followed a sequence of  $Ni > Co > Fe > Mo$ . In addition, the results of peak separation for Ni,

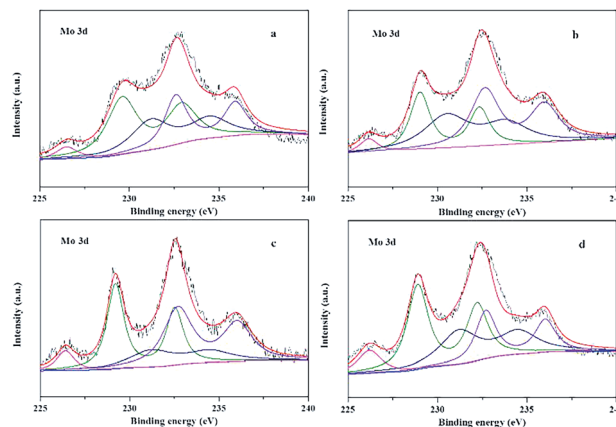


Fig. 4 XPS spectra showing the binding energies of Mo 3d in  $MoS_2/\gamma-Al_2O_3$  (a),  $Fe-MoS_2/\gamma-Al_2O_3$  (b),  $Co-MoS_2/\gamma-Al_2O_3$  (c) and  $Ni-MoS_2/\gamma-Al_2O_3$  (d) catalysts.

Co and Fe promoters in Fig. S3 (ESI<sup>†</sup>) showed that there was no obvious  $NiS_2$ ,  $CoS_2$  or  $FeS_2$  active phases formed, indicating that the single active phase could be prepared using alumina support.

The coordinative unsaturated sites (CUS) at the edge of  $MoS_2$  slabs have been deemed as the active centers in the hydrodesulfurization (HDS) and hydrodeoxygenation (HDO).<sup>48</sup> They are also postulated as the reaction sites in the selective hydrogenation of nitroarenes owing to the similar hydrogenation process. Due to NO molecule can adsorb on CUS, the NO temperature-programmed desorption (NO-TPD) experiment was used to estimate the amount of CUS on the  $MoS_2/\gamma-Al_2O_3$  and promoted  $MoS_2$  catalysts.<sup>49</sup> As shown in Fig. 5a, peak profiles were similar and the main peaks were at about 430 K, but the NO desorption capacity was different in the sequence of  $Ni > Co > Fe > Mo$ . The NO desorption capacity of  $MoS_2/\gamma-Al_2O_3$  was only  $7.5\ \mu mol\ g_{cat}^{-1}$ , NO desorption capacity of catalyst modified by Fe promoter was 2.6 times ( $19.6\ \mu mol\ g_{cat}^{-1}$ ) of the  $MoS_2/\gamma-Al_2O_3$ . Further improving the NO desorption capacity to  $28.3\ \mu mol\ g_{cat}^{-1}$  and  $33.6\ \mu mol\ g_{cat}^{-1}$  by Co and Ni promoters modified  $MoS_2$  catalysts. Fig. 5b showed the relationship between specific NO adsorption capacity and the activity of hydrogenation of nitrobenzene. The conversions of  $MoS_2/\gamma-Al_2O_3$ ,  $Fe-MoS_2/\gamma-Al_2O_3$ ,  $Co-MoS_2/\gamma-Al_2O_3$  and  $Ni-MoS_2/\gamma-Al_2O_3$  at 40 °C and 0.5 h were 16.8%, 21.5%, 25.7% and 29.6%, respectively. The NO desorption

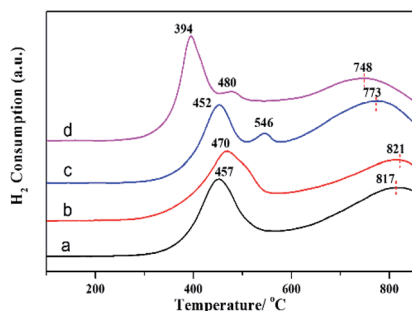


Fig. 3  $H_2$ -TPR profiles: (a)  $MoO_3/\gamma-Al_2O_3$ , (b)  $FeO_x-MoO_3/\gamma-Al_2O_3$ , (c)  $CoO_x-MoO_3/\gamma-Al_2O_3$  and (d)  $NiO_x-MoO_3/\gamma-Al_2O_3$ .

Table 2 Surface components of the various catalysts determined by XPS spectra

Samples	Mo 3d (%)			
	$Mo^{4+}$	$Mo^{5+}$	$Mo^{6+}$	$Mo^{4+} + Mo^{5+}$
$MoS_2/\gamma-Al_2O_3$	38.7	20.5	40.8	59.2
$Fe-MoS_2/\gamma-Al_2O_3$	40.5	19.5	40.0	60.0
$Co-MoS_2/\gamma-Al_2O_3$	42.5	22.4	35.1	64.9
$Ni-MoS_2/\gamma-Al_2O_3$	46.2	31.1	22.7	77.3



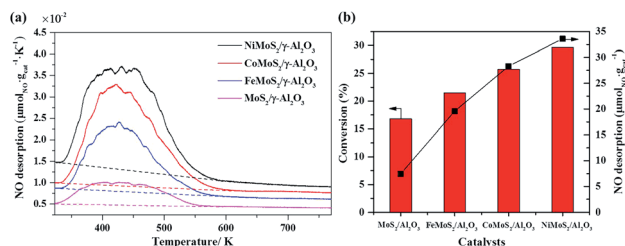


Fig. 5 (a) NO-TPD profiles of MoS<sub>2</sub>/γ-Al<sub>2</sub>O<sub>3</sub> and promoters modified catalysts; (b) the relationship between the NO desorption capacity and the conversion of nitrobenzene hydrogenation. The amount of CUS can be determined by the NO desorption data (i.e., the peak area integration). Reaction conditions: 0.1 g catalyst, 1 mmol nitrobenzene, 40 °C, 15 mL isopropyl alcohol, 1 MPa N<sub>2</sub>, 2 equiv. N<sub>2</sub>H<sub>4</sub>·H<sub>2</sub>O, 0.5 h.

capacity has a positive correlation with conversion, which indicated that the reaction activity of nitrobenzene was closely related to the amount of CUS.

### 3.3 Formation of CUS, adsorption of hydrogen and nitrobenzene as well as the reaction mechanism for hydrogenation of nitrobenzene

As reported in the literatures,<sup>34,50</sup> the nitrobenzene hydrogenation over MoO<sub>3</sub> or O-MoS<sub>2</sub> catalysts with N<sub>2</sub>H<sub>4</sub> was a transfer hydrogenation process. Wang *et al.* studied the dissociation process of N<sub>2</sub>H<sub>4</sub> on catalyst in detail by DFT calculations and the results showed that the stepwise hydrogen transfer *via* the cleavage of the N-H bond is the key step to create the dissociated hydride and active hydrogen species in polar electronic states (H<sup>δ-</sup> and H<sup>δ+</sup>). According to the above, we have a better understanding of how N<sub>2</sub>H<sub>4</sub> can release active H on the catalysts. However, there was lack of sufficient understanding of how the nitrobenzene and active H were adsorbed, reacted and desorbed on the active center. Thus, it is necessary to study the above aspects by DFT calculation. Owing to the CUS on the MoS<sub>2</sub> based catalysts is deemed as active center for selective hydrogenation of nitroarenes, we investigated the formation and regeneration of CUS by DFT calculation. To reveal the selective hydrogenation process, we studied the adsorption of hydrogen and nitrobenzene at S and Mo edges, respectively. And we investigated the consecutive six hydrogenation steps of nitrobenzene on the Ni substituted MoS<sub>2</sub> slabs. To compare the effect of promoters on the intrinsic activity, we compared the energy barrier of the rate-determining step for un-promoted and promoted MoS<sub>2</sub> catalysts.

**3.3.1 The CUS formation, hydrogen and nitrobenzene adsorption on S edge and Mo edge.** It has been well established that the hydrogenation reactions of HDS, HDN and HDO are located at the CUS on the edge of promoted or un-promoted MoS<sub>2</sub> catalysts.<sup>36</sup> The selective hydrogenation of nitrobenzene also can be seen as a hydrodeoxygenation reaction process. Thus, the active center is also suggested as the CUS on the edge. We firstly calculated the formation energy of CUS at S edge and Mo edge of MoS<sub>2</sub> slabs without promotion or with 100% Mo atoms substituted by Fe, Co and Ni respectively. The reaction of

CUS formation was presented in eqn (1), and the CUS formation energy was presented in eqn (2).

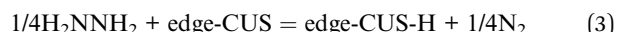


$$\Delta E_{\text{cus}} = E_{\text{edge-CUS}} + E_{\text{H}_2\text{S}} + 1/2E_{\text{N}_2} - E_{\text{edge}} + 1/2E_{\text{H}_2\text{NNH}_2} \quad (2)$$

Where the  $\Delta E_{\text{cus}}$  is the CUS formation energy,  $E_{\text{edge}}$  and  $E_{\text{edge-CUS}}$  are optimized slab energy without and with CUS respectively,  $E_{\text{H}_2\text{S}}$ ,  $E_{\text{N}_2}$  and  $E_{\text{H}_2\text{NNH}_2}$  are the energies of H<sub>2</sub>S, N<sub>2</sub> and H<sub>2</sub>NNH<sub>2</sub> in gas.

The results were listed in Table 3. It can be seen that no matter at S edge or Mo edge, the formation of CUS was favorable by the promoter substitution, and the formation energy followed the sequence of Mo > Fe > Co > Ni. In particular, Ni substituted Mo can greatly reduce the CUS formation energy from 223.7 kJ mol<sup>-1</sup> to 47.4 kJ mol<sup>-1</sup> on the S edge and from 80.8 kJ mol<sup>-1</sup> to -66.3 kJ mol<sup>-1</sup> on the Mo edge. Besides, it was found that the CUS formation energy at Mo edge was much less than that at S edge. It can be seen (Table 3) that the S coordination number of transition metal at Mo edge and S edge was six and four, respectively. The apparent unsaturation coordination property of transition metal at S edge led to the inhibition for the sulfur removal, thus the formation of CUS was more difficult. The decrease of CUS formation energy can increase the amount of CUS, facilitating the hydrogenation of nitroarenes.

In order to efficiently achieve the selective hydrogenation of nitrobenzene and derivatives, the nitrobenzene molecule needs to adsorb on CUS, meanwhile the hydrogen adsorbs on the S atom near the CUS. We thus studied the hydrogen adsorption near the CUS (Table 4). The hydrogen adsorption reaction was expressed in eqn (3), and the reaction adsorption energy calculation was shown in eqn (4).



$$\Delta E_{\text{Hads}} = E_{\text{edge-CUS-H}} + 1/4E_{\text{N}_2} - E_{\text{edge-CUS}} - 1/4E_{\text{H}_2\text{NNH}_2} \quad (4)$$

Where the  $\Delta E_{\text{Hads}}$  is the hydrogen adsorption energy,  $E_{\text{edge-CUS}}$  and  $E_{\text{edge-CUS-H}}$  are optimized slab energy without and with hydrogen adsorption near the CUS,  $E_{\text{N}_2}$  and  $E_{\text{H}_2\text{NNH}_2}$  are the energy of N<sub>2</sub> and H<sub>2</sub>NNH<sub>2</sub> in gas.

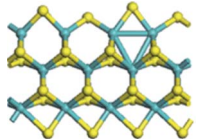
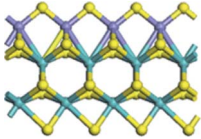
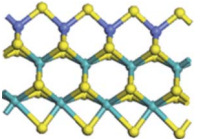
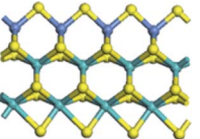
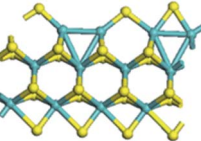
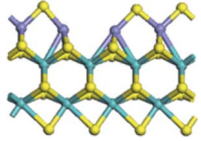
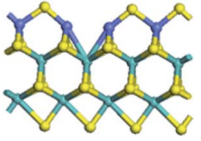
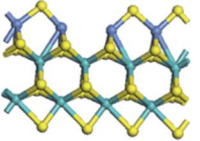
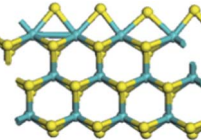
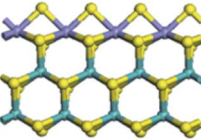
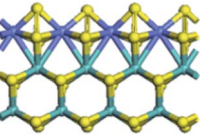
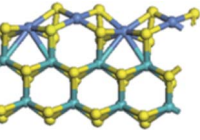
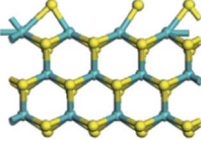
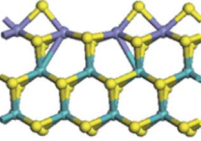
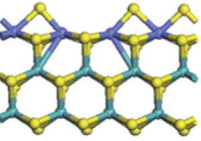
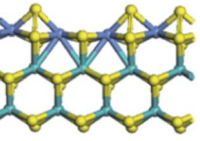
Table 4 showed the results of hydrogen adsorption reaction on the un-promoted and Fe, Co and Ni promoted S edge and Mo edge, respectively. It can be seen that the addition of promoters can apparently decrease the reaction energy of hydrogen adsorption, following a sequence of Mo > Fe > Co > Ni. No matter at S edge or Mo edge, the Ni substitution always resulted in the lowest reaction energy, illustrating that the hydrogen activation was largely facilitated by the Ni substitution of Mo at the edge. By comparison of the hydrogen adsorption at the S edge and Mo edge, it showed that hydrogen was favorable to adsorb on Mo edge than on S edge, suggesting the hydrogen was preferred to be activated at Mo edge.

Expect for the H activation is an important factor for selective hydrogenation, the activation of nitrobenzene by adsorption also plays very important roles. We further studied the adsorption energy and adsorption structure of the nitrobenzene on CUS at S edge and Mo edge for the un-promoted and





Table 3 Effect of Fe, Co and Ni promoters on formation energy of CUS

Mo substitution	No	Fe	Co	Ni
<b>S edge</b>				
CUS formation energy (kJ mol <sup>-1</sup> )	223.7	179.1	160.6	47.4
Edge				
Edge with CUS				
<b>Mo edge</b>				
CUS formation energy (kJ mol <sup>-1</sup> )	80.8	42.2	41.8	-66.3
Edge				
Edge with CUS				

promoted MoS<sub>2</sub> slabs. The adsorption energy of nitrobenzene was calculated according to eqn (5) and the adsorption structures were presented in the Table 5.

$$\Delta E_{\text{ads}} = E_{\text{CUS-nitrobenzene}} - E_{\text{CUS}} - E_{\text{nitrobenzene}} \quad (5)$$

Where the  $\Delta E_{\text{ads}}$  is the adsorption energy,  $E_{\text{CUS-nitrobenzene}}$  and  $E_{\text{CUS}}$  are energies of the optimized slab without and with nitrobenzene adsorption on CUS,  $E_{\text{nitrobenzene}}$  is the calculated energy of nitrobenzene in gas.

Table 4 Effect of Fe, Co and Ni promoters on hydrogen adsorption at S edge and Mo edge

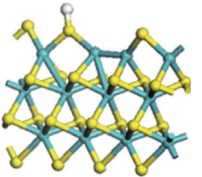
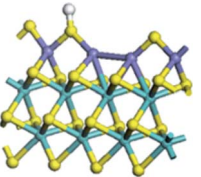
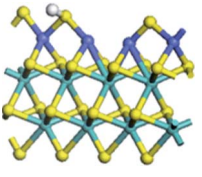
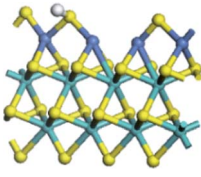
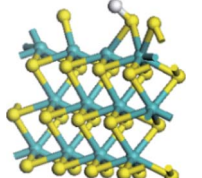
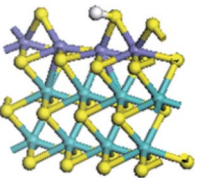
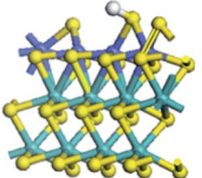
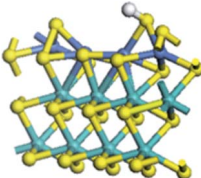
Mo substitution	No	Fe	Co	Ni
Reaction energy of H adsorption on S edge (kJ mol <sup>-1</sup> )	141.0	5.5	-8.0	-40.0
				
Reaction energy of H adsorption on Mo edge (kJ mol <sup>-1</sup> )	31.2	-40.9	-81.1	-82.7
				



Table 5 Effect of Fe, Co and Ni promoters on nitrobenzene adsorption at S edge and Mo edge

Mo substitution	No	Fe	Co	Ni
Adsorption energy on S edge ( $\text{kJ mol}^{-1}$ )	-268.9	-146.4	-87.5	-67.3
Adsorption energy on Mo edge ( $\text{kJ mol}^{-1}$ )	-43.9	7.0	-48.8	-32.9

It can be seen (Table 5) that the replacement of Mo with promoters at S edge led to the decrease of the adsorption energy of nitrobenzene, following a sequence of  $\text{Mo} > \text{Fe} > \text{Co} > \text{Ni}$ . For the adsorption conformation of nitrobenzene on un-promoted S edge, the two Mo atoms at CUS bonded with the two O atoms and the one N atom of nitro group. This may be the reason for the strongest adsorption of nitrobenzene on un-promoted S edge. For promoter promoted S edge, the nitrobenzene molecule adsorbed on CUS with two O atoms bonding with two promoter atoms, respectively. And the nitrobenzene rode on the CUS with the two O atoms located at the two sides of CUS. These results illustrated that the addition of promoter was unfavorable for the adsorption of nitrobenzene. According to the Sabatier principle, the interaction between catalyst and substrate should be no too strong nor too weak. In this work, the adsorption of nitrobenzene on the CUS can be regulated by the promoter substitution, thus influencing the intrinsic activity of hydrogenation reaction.

At Mo edge, however, the nitrobenzene hardly adsorbed on the CUS. The adsorption energies were less than  $-50 \text{ kJ mol}^{-1}$  for all four edges (negative illustrating heat release). There was a weak adsorption energy of  $-43.9 \text{ kJ mol}^{-1}$  on un-promoted CUS. Fe substitution led to a positive adsorption energy, suggesting an unfavorable adsorption. Co substituted CUS presented a weak adsorption of nitrobenzene ( $-48.8 \text{ kJ mol}^{-1}$ ) with only one O atom connected with Co atom. And for Ni substitution, the nitrobenzene only physically adsorbed on CUS with a low adsorption energy of ( $-32.9 \text{ kJ mol}^{-1}$ ). The results illustrated that the nitrobenzene cannot be effectively activated at Mo edge owing to the very weak adsorption.

Based on the above DFT results, it was postulated that the nitrobenzene and hydrogen were activated at S edge and Mo edge, respectively. Although the CUS was formed more easily on

Mo edge, the hydrogenation of nitrobenzene occurred actually on the CUS at S edge. The activated hydrogen at Mo edge diffused to S edge and participated in the hydrogenation reaction.

**3.3.2 The DFT investigation of reaction process of nitrobenzene hydrogenation.** According to the references,<sup>51,52</sup> selective hydrogenation of nitrobenzene and substituted analogs can proceed by two ways, namely direct or indirect routes. In direct route, the nitrobenzene is firstly hydrogenated to nitrosobenzene (NSB), then to hydroxylamine (PHA), and finally to aniline (AN). While in indirect route, two nitrobenzene are coupled to azoxybenzene (AOB) and azobenzene (AB), and then further hydrogenate to two aniline molecules. To determine the reaction route of  $\text{MoS}_2$  based catalysts, we performed hydrogenation experiments with nitrobenzene and four intermediates of NSB, PHA, AOB and AB as reactants and the results were shown in Table S3.† Using nitrobenzene as reactant under the given reaction conditions, the conversion was 67% (Entry 1). With NSB and PHA as reactants, the conversion increased to 95% and 99% (Entries 2 and 3), respectively. But with AOB and AB as reactants, they were hardly converted (Entries 4 and 5). These results suggested that hydrogenation reaction of nitrobenzene proceeded *via* the direct route, as revealed by the relative reported.<sup>53,54</sup> This can be reasonable that the indirect hydrogenation needs the co-adsorption of two nitrobenzene molecules on the active center, making the two nitro groups close enough to couple. However, the space of CUS in  $\text{MoS}_2$  based catalyst was too small to accommodate two bulky nitrobenzene molecules, which inhibited the combination of two nitrobenzene. In contrast, nitrobenzene molecule can adsorb on the CUS with two O atoms bonding with two promoters or Mo atoms. This adsorption led to the activation of N–O bond, decreasing the energy barrier of hydrogenation reaction. Thus,





the direct hydrogenation of nitrobenzene to aniline was favorable on the CUS active center.

Based on the above experiment and analysis, we further studied the direct reaction mechanism of nitrobenzene hydrogenation on the Ni substituted S edge. Fig. 6 presented this reaction process. For simplicity, we neglected the energy difference between the respective adsorption and the co-adsorption of H and reactant molecule, which does not influence the energy barriers of TS.<sup>55</sup> The hydrogenation of nitrobenzene proceeded six consecutive hydrogenation steps, producing two water molecules and one aniline product.<sup>54,56</sup> As shown in Fig. 6, the nitrobenzene was firstly hydrogenated to NSB, crossing energy barrier of 93.2 kJ mol<sup>-1</sup> (TS1). The NSB and PHA as intermediates were hydrogenated, passing the energy barriers of 78.0 kJ mol<sup>-1</sup> (TS2) and 54.2 kJ mol<sup>-1</sup> (TS4), respectively. These calculation results were consistent with experiment ones in Table S3.† After desorption of aniline from the CUS, only the OH group remained on the CUS (P). And the hydrogenation of OH passed a barrier of 127.7 kJ mol<sup>-1</sup> (TS5), which was the highest in the all elementary reaction. Thus for the Ni substituted S edge, the rate-determining step was suggested as the OH group hydrogenated to H<sub>2</sub>O.

To investigate the effect of promoters on the intrinsic activities of MoS<sub>2</sub> based catalysts, ones may need to calculate all the hydrogenation reaction steps over each promoted or unpromoted CUS. However, this is very expensive and daunting work. For balancing the consumption of calculation time and the effectiveness of results, we only compared energy barrier of H<sub>2</sub>O formation on the un-promoted and promoted CUS, because this reaction was the rate-determining step in the Ni substituted CUS. The results were presented in Fig. 7a. It was observed that the energy barriers increased the sequence of Fe < Ni < Mo < Co. It was deduced that CUS without promotion or with Co-promotion have higher energy barrier than Ni promoted CUS. However, Fe promoted CUS showed the lowest

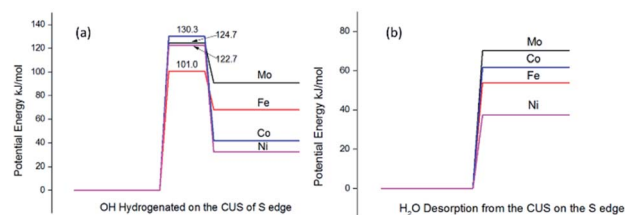


Fig. 7 Comparison of energy barrier of water formation (a) and desorption energy at CUS of S edge without promotion and with Fe, Co Ni promotion (b).

energy barrier for H<sub>2</sub>O formation. This illustrated that the observed activity for Fe promoted catalyst may not be dominated by the intrinsic activity of Fe-CUS. But there was also the other possibility, the rate-determining step on the Fe-CUS may not be the H<sub>2</sub>O formation. More detailed investigation about the reaction mechanism may be necessary for the Fe promoted surface in the future research.

The last step of hydrogenation of nitrobenzene is desorption of water, which leads to the regeneration of CUS active center. We compared the desorption energy of water on the CUS at S edge and the results were shown in Fig. 7b. It was found that desorption energy followed the sequence of Ni < Fe < Co < Mo. The promoters can facilitate the desorption of water, leading to the regeneration of promoted CUS more easily.

In this study, the catalysts were prepared with Al<sub>2</sub>O<sub>3</sub> as the support by impregnation method, which made the promoters highly dispersed and effectively adsorbed on the edge of MoS<sub>2</sub> slabs to form more the single phases such as NiMoS, CoMoS or FeMoS. The reaction activity and chemoselectivity are the most important two factors for hydrogenation of nitroarenes. It was evidenced that the addition of promoters can effectively improve the activity in the sequence of Ni > Fe > Co > Mo. The reasons can be summarized as follows:

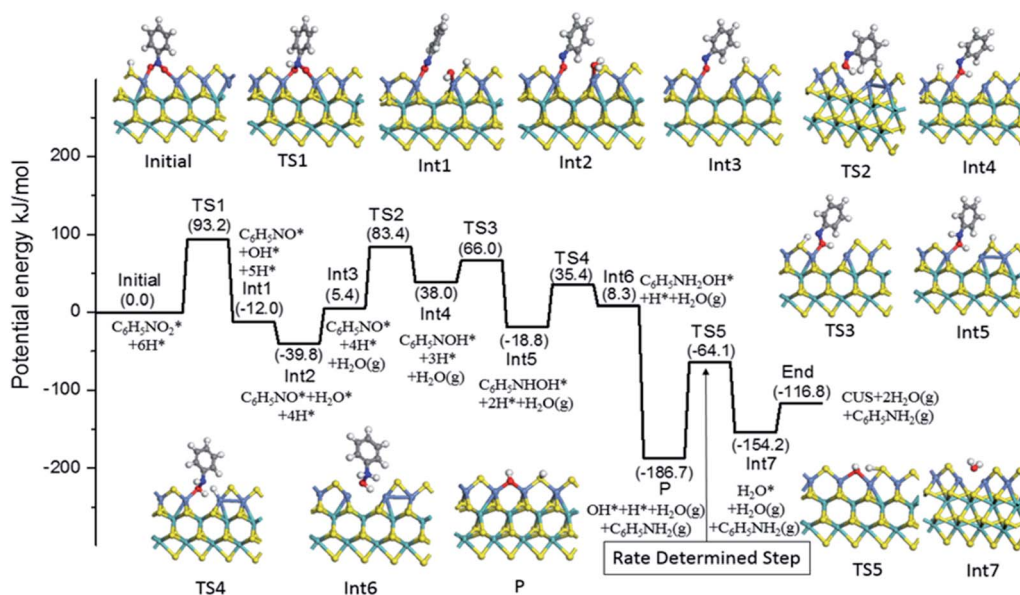


Fig. 6 Reaction profile for nitrobenzene hydrogenation at the CUS of Ni substituted S edge.

(1) The addition of Ni and Co promoters decreased the interaction between Mo with support and facilitated the reduction and sulfidation of oxide components to form more NiMoS and CoMoS active phases. However, addition of Fe promoter only slightly increased the sulfidation of Mo species, thus exhibited only a little increase of the reaction activity.

(2) The literatures reported that the NO-TPD characterization was used to measure the amount of CUS of MoS<sub>2</sub> slabs.<sup>49</sup> DFT calculation showed that NO was only the physical adsorption on the Mo edge, as shown in Table S4 (ESI†). The physical adsorbed NO will be removed by the purging treatment. Thus, the amount of NO desorption in the NO-TPD represented the CUS at S edge rather than at Mo edge. In this work, the NO-TPD measurement showed that the amount of CUS at S edge followed a sequence of Ni > Fe > Co > Mo, which was consistent with the formation of CUS at S edge by DFT calculation. Thus, the amount of CUS active center was supposed to be the main reason to influence the hydrogenation activity.

(3) The addition of promoters can facilitate the formation of type II active phases, which possessed the higher intrinsic activities. This can be another reason for the improved reaction activities.

(4) The addition of promoters was favorable for the hydrogen activation. The hydrogen may firstly adsorb activation on the Mo edge. Due to that supported MoS<sub>2</sub> was hexagon slab with the S edge and Mo edge arrayed alternatively, the adsorbed hydrogen can diffuse from the Mo edge to S edge through the corner.

(5) The addition of Ni promoter showed the weakest adsorption of nitrobenzene, but the strongest adsorption of hydrogen. The un-promoted catalyst showed the strongest adsorption of nitrobenzene, but the weakest adsorption of hydrogen, and Co and Fe were between them. The synergy effect of adsorption of nitrobenzene and hydrogen mainly influenced the intrinsic activity. The comparison of energy barrier of H<sub>2</sub>O formation showed that CUS without promotion or with Co-promotion have lower catalytic intrinsic activities than Ni promoted CUS. Interestingly, Fe promoted CUS showed the lowest energy barrier for H<sub>2</sub>O formation, even though the H<sub>2</sub>O formation may not be the rate determined step of the reaction. As we known, Fe based catalysts have showed excellent performance for hydrogenation of the nitroarenes. Therefore, Fe promoted MoS<sub>2</sub> catalyst may also have high intrinsic activity, but it may be affected by the preparation method and sulfidation, which made the observed activity lower.

As for the hydrogenation selectivity of the catalysts, due to that the nitro group can ride on the CUS with the two O atoms bonding with the transition metal, the N–O bond can be sufficiently activated, leading that the hydrodeoxygenation of nitro group became easier. This concerted combination of nitro group with CUS does not appear for most of other sensitive groups. Thus the high selectivity of MoS<sub>2</sub> based catalysts can be obtained. Another reason is that nitro group is usually more easily hydrogenated than other sensitive groups. The substitution of Mo with promoter atoms mainly change the electronic structures, but does not apparently change the geometry structures. Thus the reaction activities are heavily influenced, however, the selectivity is less influenced. As a result, the MoS<sub>2</sub> based catalysts can achieve the good chemoselectivity for hydrogenation of nitroarenes.

## 4 Conclusions

By the impregnation method, Fe, Co and Ni promoters modified MoS<sub>2</sub> catalysts were prepared and employed for the hydrogenation of nitroarenes. The addition of promoters remarkably improved the reaction activity in a sequence of Ni > Co > Fe > Mo. And Ni promoted catalyst with the best performance also showed good recyclability and chemoselectivity for many substrates with sensitive groups such as nitrile, ketone, alkenyl and so on. Characterization results showed that the active particles were highly dispersed and promoter modification decreased the interaction between Mo with support, which facilitated the formation of type II active phases with higher intrinsic activity. Addition of Fe promoter only slightly improved the sulfidation of Mo species compared with the sulfidation of MoS<sub>2</sub>/γ-Al<sub>2</sub>O<sub>3</sub>. However, the addition of Co and Ni promoters can apparently promote the reduction of Mo species, so that the sulfidation of Mo species was remarkably improved, especially for Ni promoter. NO-TPD measurement showed that the amount of CUS active center followed a sequence of Ni > Co > Fe > Mo. The DFT calculations revealed that the nitrobenzene and hydrogen were activated at S edge and Mo edge, respectively. The hydrogenation of nitrobenzene occurred on CUS at S edge, and activated hydrogen at Mo edge diffused to S edge to participate in the hydrogenation reaction. For Ni promoted MoS<sub>2</sub> surface, the H<sub>2</sub>O formation in the second last step has the highest TS barrier, suggested as the rate-determining step. The formed water was easier to release from CUS active center for promoter modification, which made the CUS active center regenerated more efficiently. The present studies give a new understanding for the promoter modified MoS<sub>2</sub> catalysts applied for the hydrogenation of nitroarenes.

## Conflicts of interest

There are no conflicts to declare.

## Acknowledgements

This work was supported financially by the National Natural Science Foundation of China (No. 21473231 and No. 21603256).

## Notes and references

- 1 R. S. Downing, P. J. Kunkeler and H. van Bekkum, *Catal. Today*, 1997, **37**, 121–136.
- 2 J. J. Song, Z. F. Huang, L. Pan, K. Li, X. W. Zhang, L. Wang and J. J. Zou, *Appl. Catal., B*, 2018, **227**, 386–408.
- 3 M. Macino, A. J. Barnes, R. Y. Qu, E. K. Gibson, D. J. Morgan, S. J. Freakley, N. Dimitratos, C. J. Kiely, X. Gao, A. M. Beale, D. Bethell, Q. He, M. Sankar, G. J. Hutchings and S. M. Althabhan, *Nat. Catal.*, 2019, **2**, 873–881.
- 4 P. Lara and K. Philippot, *Catal. Sci. Technol.*, 2014, **4**, 2445–2465.
- 5 S. Giri, R. Das, C. van der Westhuyzen and A. Maity, *Appl. Catal., B*, 2017, **209**, 669–678.



- 6 R. Sedghi, M. M. Heravi, S. Asadi, N. Nazari and M. R. Nabid, *Curr. Org. Chem.*, 2016, **20**, 696–734.
- 7 A. Corma and P. Serna, *Science*, 2006, **313**, 332–334.
- 8 F. Q. Leng, I. C. Gerber, P. Lecante, S. Moldovan, M. Girleanu, M. R. Axet and P. Serp, *ACS Catal.*, 2016, **6**, 6018–6024.
- 9 T. W. He, C. M. Zhang, L. Zhang and A. J. Du, *Nano Res.*, 2019, **12**, 1817–1823.
- 10 J. J. Shi, Y. Y. Wang, W. C. Du and Z. Y. Hou, *Carbon*, 2016, **99**, 330–337.
- 11 R. V. Jagadeesh, A. E. Surkus, H. Junge, M. M. Pohl, J. Radnik, J. Rabeah, H. M. Huan, V. Schunemann, A. Bruckner and M. Beller, *Science*, 2013, **342**, 1073–1076.
- 12 Z. Z. Wei, J. Wang, S. J. Mao, D. F. Su, H. Y. Jin, Y. H. Wang, F. Xu, H. R. Li and Y. Wang, *ACS Catal.*, 2015, **5**, 4783–4789.
- 13 F. W. Zhang, C. Zhao, S. Chen, H. Li, H. Q. Yang and X. M. Zhang, *J. Catal.*, 2017, **348**, 212–222.
- 14 H. G. Huang, X. C. Liang, X. G. Wang, Y. Sheng, C. J. Chen, X. J. Zou and X. G. Lu, *Appl. Catal., A*, 2018, **559**, 127–137.
- 15 W. C. Cheong, W. J. Yang, J. Zhang, Y. Li, D. Zhao, S. J. Liu, K. L. Wu, Q. G. Liu, C. Zhang, D. S. Wang, Q. Peng, C. Chen and Y. D. Li, *ACS Appl. Mater. Interfaces*, 2019, **11**, 33819–33824.
- 16 W. She, T. Q. J. Qi, M. X. Cui, P. F. Yan, S. W. Ng, W. Z. Li and G. M. Li, *ACS Appl. Mater. Interfaces*, 2018, **10**, 14698–14707.
- 17 G. Hahn, J. K. Ewert, C. Denner, D. Tilgner and R. Kempe, *ChemCatChem*, 2016, **8**, 2461–2465.
- 18 M. Y. Li, V. Bacic, I. A. Popov, A. I. Boldyrev, T. Heine, T. Frauenheim and E. Ganz, *J. Am. Chem. Soc.*, 2015, **46**, 2757–2762.
- 19 J. H. Liu, L. M. Yang and E. Ganz, *J. Mater. Chem. A*, 2019, **7**, 11944–11952.
- 20 J. H. Liu, L. M. Yang and E. D. Ganz, *J. Mater. Chem. A*, 2019, **7**, 3805–3814.
- 21 J. H. Liu, L. M. Yang and E. Ganz, *Energy Environ. Sci.*, 2019, **2**, 193–200.
- 22 P. Zhao, Y. D. Ma, X. S. Lv, M. M. Li, B. B. Huang and Y. Dai, *Nano Energy*, 2018, **51**, 533–538.
- 23 J. R. Morse, J. F. Callejas, A. J. Darling and R. E. Schaak, *Chem. Commun.*, 2017, **53**, 4807–4810.
- 24 Y. N. Zhang, X. H. Li, Y. Y. Cai, L. H. Gong, K. X. Wang and J. S. Chen, *RSC Adv.*, 2014, **4**, 60873–60877.
- 25 B. Ma, X. L. Tong, C. X. Guo, X. N. Guo, X. Y. Guo and F. J. Keil, *RSC Adv.*, 2016, **6**, 55220–55224.
- 26 B. Ma, Y. Y. Wang, X. L. Tong, X. N. Guo, Z. F. Zheng and X. Y. Guo, *Catal. Sci. Technol.*, 2017, **7**, 2805–2812.
- 27 Z. Z. Wei, S. J. Mao, F. F. Sun, J. Wang, B. B. Mei, Y. Q. Chen, H. R. Li and Y. Wang, *Green Chem.*, 2018, **20**, 671–679.
- 28 Y. N. Duan, X. S. Dong, T. Song, Z. Z. Wang, J. L. Xiao, Y. Z. Yuan and Y. Yang, *ChemSusChem*, 2019, **12**, 4636–4644.
- 29 S. Garcia-Dali, J. I. Paredes, J. M. Munuera, S. Villar-Rodil, A. Adawy, A. Martinez-Alonso and J. M. D. Tascon, *ACS Appl. Mater. Interfaces*, 2019, **11**, 36991–37003.
- 30 N. Saha, A. Sarkar, A. B. Ghosh, A. K. Dutta, G. R. Bhadu, P. Paul and B. Adhikary, *RSC Adv.*, 2015, **5**, 88848–88856.
- 31 Z. C. Li, D. L. Zhang, J. J. Ma, D. B. Wang and C. X. Xie, *Mater. Lett.*, 2018, **213**, 350–353.
- 32 L. Huang, P. F. Luo, M. Xiong, R. Z. Chen, Y. Wang, W. H. Xing and J. Huang, *Chin. J. Chem.*, 2013, **31**, 987–991.
- 33 C. F. Zhang, X. Wang, M. R. Li, Z. X. Zhang, Y. H. Wang, R. Si and F. Wang, *Chin. J. Catal.*, 2016, **37**, 1569–1578.
- 34 C. F. Zhang, Z. X. Zhang, X. Wang, M. R. Li, J. M. Lu, R. Si and F. Wang, *Appl. Catal., A*, 2016, **525**, 85–93.
- 35 J. Wang, Y. J. Zhang, J. Y. Diao, J. Y. Zhang, H. Y. Liu and D. S. Su, *Chin. J. Catal.*, 2018, **39**, 79–87.
- 36 H. Topsøe, B. S. Clausen, R. Candia, C. Wivel and S. Morup, *J. Catal.*, 1981, **68**, 433–452.
- 37 Y. L. Jia, Z. H. Wang, L. Y. Wang, Y. Ma, G. N. Wang, Y. H. Lin, X. Hu and K. Zhang, *ChemSusChem*, 2019, **12**, 3336–3342.
- 38 I. Sorribes, L. C. Liu and A. Corma, *ACS Catal.*, 2017, **7**, 2698–2708.
- 39 C. Nethravathi, J. Prabhu, S. Lakshmipriya and M. Rajamathi, *ACS Omega*, 2017, **2**, 5891–5897.
- 40 G. Shi, W. Han, P. Yuan, Y. Fan and X. J. Bao, *Chin. J. Catal.*, 2013, **34**, 659–666.
- 41 S. Texier, G. Berhault, G. Perot, V. Harle and F. Diehl, *J. Catal.*, 2004, **223**, 404–418.
- 42 P. Zheng, T. S. Li, K. B. Chi, C. K. Xiao, J. Y. Fan, X. L. Wang and A. J. Duan, *Appl. Catal., B*, 2019, **257**, 11.
- 43 F. Caron, M. Rivallan, S. Humbert, A. Daudin, S. Bordiga and P. Raybaud, *J. Catal.*, 2018, **361**, 62–72.
- 44 M. Y. Sun, A. E. Nelson and J. Adjaye, *J. Catal.*, 2005, **233**, 411–421.
- 45 A. S. Nagpure, A. K. Venugopal, N. Lucas, M. Manikandan, R. Thirumalaiswamy and S. Chilukuri, *Catal. Sci. Technol.*, 2015, **5**, 1463–1472.
- 46 H. Ge, X.-D. Wen, M. A. Ramos, R. R. Chianelli, S. Wang, J. Wane, Z. Qin, Z. Lyu and X. Li, *ACS Catal.*, 2014, **4**, 2556–2565.
- 47 Y. R. Liu, X. Shang, W. K. Gao, B. Dong, J. Q. Chi, X. Li, K. L. Yan, Y. M. Chai, Y. Q. Liu and C. G. Liu, *Appl. Surf. Sci.*, 2017, **412**, 138–145.
- 48 S. M. Wang, H. Ge, W. P. Han, Y. J. Li, J. Z. Zhang, X. H. Yu, J. Q. Qin, Z. W. Quan, X. D. Wen, X. K. Li, L. P. Wang, L. L. Daemen, D. W. He and Y. S. Zhao, *J. Phys. Chem. C*, 2017, **121**, 19451–19460.
- 49 P. Liu, J. C. Lu, Z. Z. Xu, F. Liu, D. K. Chen, J. Yu, J. P. Liu, S. F. He, G. P. Wan and Y. M. Luo, *Mol. Catal.*, 2017, **442**, 39–48.
- 50 C. F. Zhang, J. M. Lu, M. R. Li, Y. H. Wang, Z. Zhang, H. J. Chen and F. Wang, *Green Chem.*, 2016, **18**, 2435–2442.
- 51 H. U. Blaser, *Science*, 2006, **313**, 312–313.
- 52 X. C. Meng, H. Y. Cheng, S. Fujita, Y. C. Yu, F. Y. Zhao and M. Arai, *Green Chem.*, 2011, **13**, 570–572.
- 53 A. Mahata, R. K. Rai, I. Choudhuri, S. K. Singh and B. Pathak, *Phys. Chem. Chem. Phys.*, 2014, **16**, 26365–26374.
- 54 R. Milian, L. C. Liu, M. Boronat and A. Corma, *J. Catal.*, 2018, **364**, 19–30.
- 55 T. Sheng, Y. J. Qi, X. Lin, P. Hu, S. G. Sun and W. F. Lin, *Chem. Eng. J.*, 2016, **293**, 337–344.
- 56 L. Gong, Y. Mu and M. J. Janik, *Appl. Catal., B*, 2018, **236**, 509–517.

